Optics Letters

Efficient nonlinear compression of a thin-disk oscillator to 8.5 fs at 55 W average power

Gaia Barbiero,[1,2] Haochuan Wang,[1,2] Martin Graßl,[1] Sebastian Gröbmeyer,[1] Džiugas Kimbaras,[1] Marcel Neuhaus,[1,2] Vladimir Pervak,[1] Thomas Nubbemeyer,[1,2] Hanieh Fattahi,[3] and Matthias F. Kling[1,2,*]

[1]Department of Physics, Ludwig-Maximilians-Universität Munich, Am Coulombwall 1, D-85748 Garching, Germany
[2]Max Planck Institute of Quantum Optics, Hans-Kopfermann-Str. 1, D-85748 Garching, Germany
[3]Max Planck Institute for the Science of Light, Staudtstraße 2, D-91058 Erlangen, Germany
*Corresponding author: matthias.kling@mpq.mpg.de

Received 16 August 2021; revised 27 September 2021; accepted 1 October 2021; posted 1 October 2021 (Doc. ID 440303); published 19 October 2021

We demonstrate an efficient hybrid-scheme for nonlinear pulse compression of high-power thin-disk oscillator pulses to the sub-10 fs regime. The output of a home-built, 16 MHz, 84 W, 220 fs Yb:YAG thin-disk oscillator at 1030 nm is first compressed to 17 fs in two nonlinear multipass cells. In a third stage, based on multiple thin sapphire plates, further compression to 8.5 fs with 55 W output power and an overall optical efficiency of 65% is achieved. Ultrabroadband mid-infrared pulses covering the spectral range 2.4-8 μm were generated from these compressed pulses by intra-pulse difference frequency generation.

https://doi.org/10.1364/OL.440303

Nowadays, few-cycle pulses are routinely generated from state-of-the-art high-power, high-energy ultrafast laser amplifier systems by using parametric amplification [1,2] combined with nonlinear compression in noble-gas-filled hollow capillaries [3–5], multipass cells [6,7], or multiplate arrangements [8–10]. Such amplifier-based few-cycle systems are, however, usually complex, costly, and typically limited to kHz repetition rates. While high-power multi-MHz repetition-rate systems have great potential to enhance (time-resolved) spectroscopic applications, efficient compression schemes for reaching below 10 fs are lacking. Promising applications for such systems include single-pass [11] or resonator-enhanced [12] extreme-ultraviolet generation [13], terahertz [14,15], and mid-infrared (MIR) generation [16]. Kerr-lens mode-locked (KLM) Yb:YAG thin-disk (TD) oscillators with their ability to deliver more than 100 W average power with pulse durations below 200 fs combine high peak and high-average powers in a relative compact setup [17]. The narrow bandwidth of the gain medium, however, limits the direct use of these powerful sources in ultrafast spectroscopy applications [18]. Efficient extra-cavity broadening remains key toward applications that demand ultrashort pulses.

Various approaches utilizing self-phase modulation (SPM) have been employed to overcome the limited bandwidth of KLM Yb:YAG TD oscillators. Gas-filled Kagomè photonic-crystal fibers (PCFs) offer an efficient way for temporal pulse compression and were shown to yield 9.1 fs with 14.5 W average power in two subsequent stages [19]. This approach, however, showed increased susceptibility to damage at high-average and peak powers. Additionally, fibers are alignment sensitive and couple pointing-drifts to laser-power fluctuations. Broadening in multiple plates of bulk material [20,21] proved to be a valuable alternative for reaching down to 17 fs. Here, the nonlinear distortion of the beam caused by self-focusing led to a degradation of the beam quality after two stages of bulk media and required additional spatial filtering, limiting the achievable throughput efficiency [20]. In recent years, efficient and robust compression of KLM-Yb:YAG TD oscillators with multipass cells [14,22–25] was demonstrated. Multipass cells consist of focusing elements (concave dispersive mirrors) and a nonlinear medium into which the beam is imaged several times. The damage threshold of the optical elements and the requirement of accurate dispersion compensation over a large spectral bandwidth, however, limited this approach to the generation of 15 fs pulses [25]. For further compression toward even shorter pulse duration, a different broadening and compression scheme is required.

In this work, we implement a hybrid compression scheme for KLM-Yb:YAG TD oscillators, combining two different approaches in sequence: two multipass cells followed by a multiplate compression stage. A similar approach with a multipass cell and multiplate arrangement has been used to compress a mode-locked TD oscillator to 27 fs at 98 W [26]. Here, we demonstrate compression of 220 fs pulses with 84 W from a KLM-Yb:YAG TD oscillator at 1030 nm to the sub-10 fs regime with high optical efficiency of 65%. One typical application of such a few-cycle near-infrared (NIR) driving source with high peak power is the generation of broadband carrier-envelope phase (CEP) stable MIR pulses by intra-pulse difference frequency generation (iDFG) [27,28]. Since the shortest wavelength in the generated iDFG output is achieved

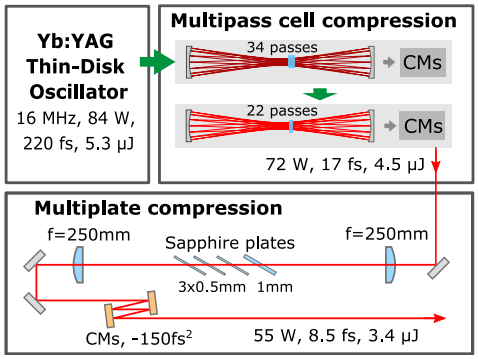

Fig. 1. Schematic of the hybrid-nonlinear compression setup. CMs, chirped mirrors.

by mixing the outer wings of the driving laser spectrum, using ultrashort driving pulses enables generating MIR radiation in the short-wavelength region. In a proof-of-principle study, the compressed high-power few-cycle pulses demonstrated here were employed in iDFG in $LiIO_3$, resulting in a broadband CEP-stable MIR continuum spanning the 2.4-8 µm spectral range.

The layout of the experimental setup is shown in Fig. 1. The driving laser is a high-power KLM-Yb:YAG TD oscillator, delivering 100 W average power at 16 MHz repetition rate with a pulse duration of 220 fs [29]. While 16 W of the output power was split off for other experiments, the residual 84 W of the oscillator output was compressed to 17 fs in two consecutive Herriott-type multipass cells, similar to those depicted in [15]. Spreading the nonlinear phase shift over two multipass cells followed by chirped mirror compressors gave the best compression results. The first multipass cell is based on two curved dispersive mirrors with a radius of curvature (ROC) of 300 mm, and group delay dispersion (GDD) of $-110\ \mathrm{fs}^2$ for 200 nm spectral bandwidth centered at 1030 nm. A 6.35-mm-thick, anti-reflection (AR)-coated fused silica (FS) plate is used as the nonlinear medium. After 34 passes through the medium, the beam is coupled out and compressed to 49 fs by eight bounces on chirped mirrors with a total GDD of $-2400\ \mathrm{fs}^2$. The second multipass cell is based on two curved dispersive mirrors with ROC of 300 mm and GDD of $-60\ \mathrm{fs}^2$ for 450 nm spectral bandwidth centered at 1030 nm. A 3-mm-thick, AR-coated FS plate is used as the nonlinear medium. After 22 passes through the medium, the beam is coupled out and compressed to 17 fs, close to the Fourier limit (16 fs), with two bounces on chirped mirrors with a total GDD of $-220\ \mathrm{fs}^2$.

Our hybrid compression scheme includes an additional stage for reaching the sub-10 fs regime: multiplate continuum generation in thin sapphire plates. As shown in Fig. 1, four uncoated sapphire plates are placed after the focus of a lens with $f = 250$ mm. The plate thicknesses are 1 mm for the first plate and 0.5 mm for the other three plates, respectively. After the plates, the beam is re-collimated by another lens and sent to a chirped mirror compressor with a total GDD of $-150\ \mathrm{fs}^2$.

As with other types of continuum generation setups [14,22–25], SPM is the main effect exploited to achieve spectral broadening, but the nonlinear phase shift per plate was kept limited such that the spatial and temporal quality of the input beam was maintained after the plates [8,30]. For the multiplate continuum setup described in this work, the peak intensity required for SPM is maintained by a reduction of the beam size

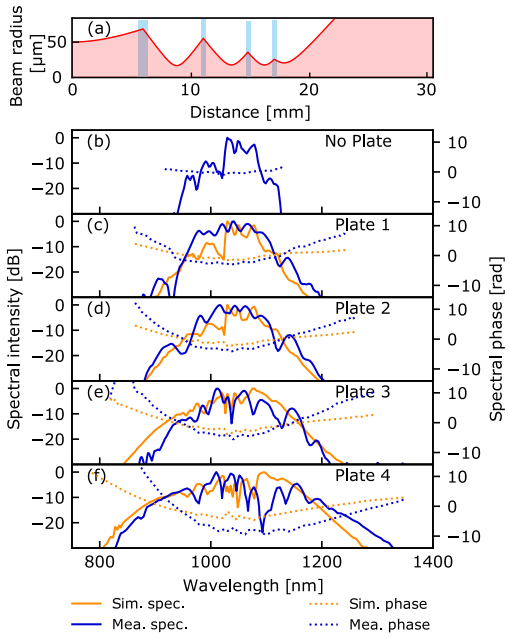

Fig. 2. (a) Caustic of the input beam along the plates obtained from simulations with *ReZonator2* [31]. The origin of the x axis lies at the focus of the input lens. FROG retrieved (blue) spectra with spectral phase (b) for the input pulse, and (c)–(f) after passage through each of the thin plates. Simulated (orange) spectra with spectral phase employing the Python package PyNLO [32] are shown for comparison.

on successive plates, induced by self-focusing within each plate. The simulated caustic of the self-focused beam was modeled analytically with the *ReZonator2* software [31] and is shown in Fig. 2(a), demonstrating the beam size reduction for consecutive plates.

At the front surface of each plate, the beam is actually divergent with the self-focus located after the back surface. The limit of this multiplate continuum setup is reached when the self-focusing-induced reduction of beam size does not suffice anymore to compensate the reduction of the peak intensity by material-induced dispersion and SPM-induced pulse stretching in the time domain.

Different parameters have to be taken into account for the design of the multiplate continuum setup. (i) The material should offer a high nonlinear refractive index and high damage threshold for maximum broadening. Four different materials have been tested: FS, quartz, YAG, and sapphire. With sapphire, the broadest spectrum was achieved without damaging the plate. (ii) The thickness of each plate not only determines SPM but also the induced self-focusing and, thus, the beam size for the subsequent plate. (iii) The beam size on the front surface of each plate is determined by its position with respect to the lens and previous plate(s).

Different combinations of sapphire plates with thicknesses ranging from 0.25 mm to 5 mm have been tested. The largest spectral broadening is achieved with a divergent input beam. The higher the divergence, the higher the required positioning precision is for the next plate along the beam path. This is a consequence of the smaller distance between the two beam radii where the intensity is sufficient for self-focusing and where the

intensity is below the damage threshold of the plate. The μJ-level pulse energy after the multipass cells implied a small beam diameter on the order of 100 μm for sufficient self-focusing. For this reason, each plate is placed close to the focus, and the relative distances between the plates remain very small, on the order of 5 mm. This strongly limited the space between the plates. Therefore, all plates had to be positioned at the same Brewster angle and not at complementary Brewster angles as in, e.g., [10].

The focal length of the input lens was chosen to be 250 mm, and the best broadening result after the first plate was obtained with a 1-mm-thick sapphire plate, where damage of the plate only occurs at the focus. The subsequent plates are positioned as follows: each plate is placed after the focus and then moved toward the focus until the highest broadening is reached without damaging the plate or distortions of the output beam. The divergent beam after the last plate is then re-collimated by an identical lens ($f = 250$ mm). The material dispersion of the plates stretches the pulses to 80 fs, and we find that adding any additional plate did not show further spectral broadening. The output beam is re-compressed by four bounces on chirped mirrors with a total GDD of -150 fs^2. The total optical efficiency of the multiplate continuum generation stage including the chirped mirrors is 80%.

The effect of each plate with respect to spectral broadening and phase is shown in blue in Figs. 2(b)–2(f). The spectral broadening was simulated by solving the nonlinear Schrödinger equation using the fourth-order Runge–Kutta in the Interaction Picture (RK4IP) method within the Python package PyNLO [32], assuming constant beam diameters within the plates. The comparisons of simulated (orange) and experimental (blue) spectra in Figs. 2(b)–2(f) show good agreement up to the third plate. After this point, deviations between experimental data and simulations become obvious. Here, careful full-field 4D simulations taking into account spatiotemporal coupling would be required [33], which were outside the scope of this work.

The compressed pulses after the chirped mirrors are characterized by second-harmonic frequency resolved optical gating (SH-FROG), employing a 10-μm-thick beta-barium borate crystal. The measured and retrieved spectrograms, the measured and retrieved spectra, and the temporal profile are shown in Figs. 3(a)–3(d). The temporal profile shows that the pulses are re-compressed to 8.5 fs (FWHM), close to the Fourier limit of 8.1 fs, with 64.3% of the energy contained in the main peak. We also found high power and beam pointing stabilities after the multiplate setup. The average power root-mean-square (RMS) fluctuations are only 0.17% over 1 h [cf. Fig. 3(e)]. The RMS beam pointing fluctuations are 0.7% within 1 h. The beam quality remained similar, with M^2 values of 1.24 and 1.10, in x and y directions, respectively, for the input beam and corresponding values of 1.29 and 1.40 for the output beam (ISO 11146 measured with M^2-200s, Ophir-Spiricon LLC).

As a simple approach to generate broadband MIR pulses, iDFG driven by femtosecond pulses [27,34] has intrinsic CEP-stability yielding highly reproducible MIR waveforms. Here, we demonstrate that the compressed 8.5 fs pulses from our oscillator system can generate an MIR continuum spanning from 2.4 to 8 μm.

As depicted in Fig. 4(a), the 8.5 fs pulses are focused into a $LiIO_3$ crystal with an $f = 300$ mm lens. The crystal is oriented to evenly distribute the p-polarized input pulses along the extraordinary and the ordinary axes for type I phase matching. The generated MIR radiation is separated by a tailored ZnSe beam splitter (UltraFast Innovations GmbH, F3-S161108) and then re-collimated by a gold-coated off-axis parabolic mirror with focal length of 101.6 mm. A 2400-nm long-pass filter is used to remove the residual pump radiation transmitted through the beam splitter. After the long-pass filter the MIR radiation is characterized by a powermeter and a monochromator (Newport, Cornerstone 260).

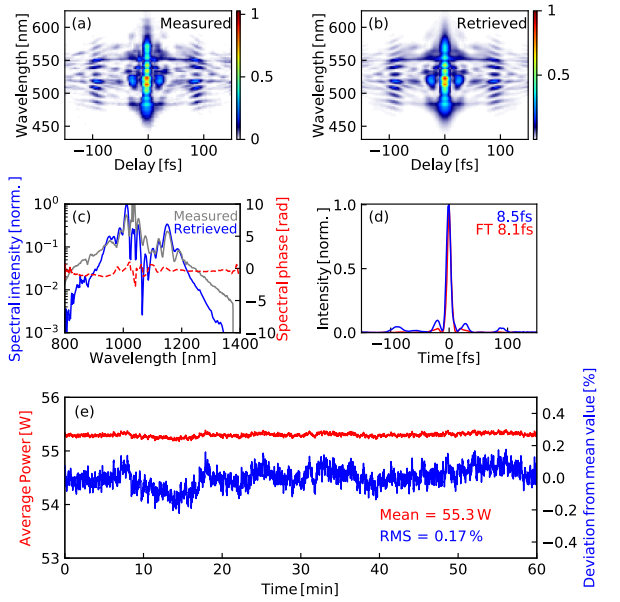

Fig. 3. Temporal and power stability characterization of the multiplate continuum setup. (a) Measured and (b) retrieved SH-FROG spectrograms of the multiplate continuum setup after the subsequent chirped mirror compressor (grid size, 512×512 points; G-error = 0.67%). (c) Measured and retrieved spectrum of the broadened pulses. The red dashed line represents the spectral phase. (d) Retrieved temporal profile of the compressed pulse. (e) Average power stability measured over 1 h with 1 Hz sampling frequency.

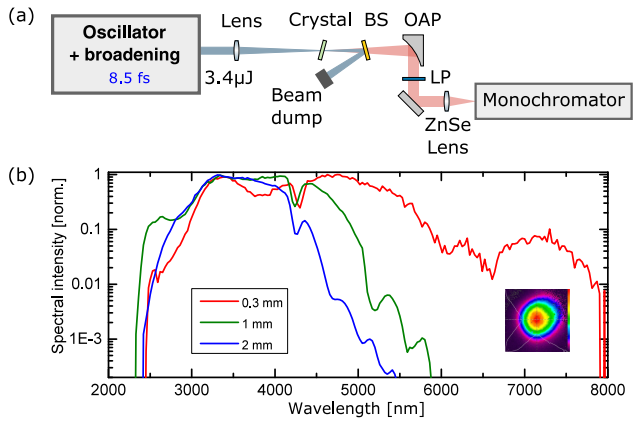

Fig. 4. Broadband short-range MIR generation by iDFG. (a) Schematic of MIR generation and characterization setup. (b) The generated MIR spectrum in 0.3 mm, 1 mm, and 2 mm $LiIO_3$ crystals. Inset, measured beam profile after 2 mm crystal and a 2400-nm long-pass filter (LP2400-33-969, Edmund Optics Ltd.). BS, beam splitter; OAP, off-axis parabola; LP, long-pass filter.

The crystals (EKSMA Optics, UAB) used in this work had broadband AR coatings for the incident NIR light and different thicknesses: 2 mm, 1 mm, and 0.3 mm. The highest average powers measured before damage of the crystal were 72 mW, 16 mW, and 1.1 mW, respectively, using the same input power of 55 W. The corresponding iDFG spectra are shown in Fig. 4(b). To suppress second-order diffraction of the monochromator, three long-pass filters with cut-on wavelengths at 2.4, 4.5, and 7.3 μm were used, and the spectra merged [28]. For the 0.3 mm crystal, the spectral coverage spanned almost two octaves, from 2.4 μm to 8 μm within a 10^{-3} dynamic range. While in previous iDFG experiments driven by KLM-Yb:YAG TD oscillators with 16 fs pulses only wavelengths down to 3 μm could be covered [28], the current results extend the spectral coverage down to 2.4 μm.

In conclusion, an efficient hybrid compression scheme for KLM-Yb:YAG TD oscillators was demonstrated. The setup consisted of two consecutive multipass cells and a multiplate continuum generation stage. With an overall efficiency of 65%, we achieved 8.5 fs pulses at 16 MHz with 55 W average power and excellent long-term power and beam pointing stabilities with a relatively simple setup. The generated few-cycle pulses open up many applications, such as the generation of ultrabroadband MIR radiation for time-resolved spectroscopy. We showed that iDFG in $LiIO_3$ resulted in a broadband MIR continuum spanning from 2.4 to 8 μm. The high repetition rate, combined with the high intensity and the remarkable stability of the overall laser system, paves the way for future applications that require high intensities, such as further spectral broadening, broadband frequency up/downconversion, and new applications in ultrafast spectroscopy.

Funding. Max-Planck-Gesellschaft (IMPRS-APS, Max Planck Fellow program, MPSP); Deutsche Forschungsgemeinschaft (LMUexcellent).

Acknowledgment. We are grateful to Ferenc Krausz for his support and for providing suitable laboratory space. We acknowledge help from Jonathan Brons for his support regarding the oscillator, and Kafai Mak and Alexander Weigel for useful discussions and proofreading. G.B., H.W., and D.K. are grateful for support from the International Max Planck Research School on Advanced Photon Science (IMPRS-APS). D.K. and M.F.K. acknowledge support from the Max Planck School of Photonics (MPSP), and M.F.K. is grateful for support from the Max Planck Society within their Max Planck Fellow program.

Disclosures. The authors declare no conflicts of interest.

Data Availability. Data underlying the results presented in this Letter are not publicly available at this time but may be obtained from the authors upon reasonable request.

REFERENCES

1. R. Budriūnas, T. Stanislauskas, J. Adamonis, A. Aleknavičius, G. Veitas, D. Gadonas, S. Balickas, A. Michailovas, and A. Varanavičius, Opt. Express **25**, 5797 (2017).
2. K. Mecseki, M. K. Windeler, A. Miahnahri, J. S. Robinson, J. M. Fraser, A. R. Fry, and F. Tavella, Opt. Lett. **44**, 1257 (2019).
3. T. Nagy, S. Hädrich, P. Simon, A. Blumenstein, N. Walther, R. Klas, J. Buldt, H. Stark, S. Breitkopf, P. Jójárt, I. Seres, Z. Várallyay, T. Eidam, and J. Limpert, Optica **6**, 1423 (2019).
4. Y.-G. Jeong, R. Piccoli, D. Ferachou, V. Cardin, M. Chini, S. Hädrich, J. Limpert, R. Morandotti, F. Légaré, B. E. Schmidt, and L. Razzari, Sci. Rep. **8**, 11794 (2018).
5. G. Fan, P. Carpeggiani, Z. Tao, G. Coccia, R. Safaei, E. Kaksis, A. Pugzlys, F. Légaré, B. Schmidt, and A. Baltuška, Opt. Lett. **46**, 896 (2021).
6. P. Balla, A. B. Wahid, I. Sytcevich, C. Guo, A.-L. Viotti, L. Silletti, A. Cartella, S. Alisauskas, H. Tavakol, U. Grosse-Wortmann, A. Schönberg, M. Seidel, A. Trabattoni, B. Manschwetus, T. Lang, F. Calegari, A. Couairon, A. L'Huillier, C. L. Arnold, I. Hartl, and C. M. Heyl, Opt. Lett. **45**, 2572 (2020).
7. M. Müller, J. Buldt, H. Stark, C. Grebing, and J. Limpert, Opt. Lett. **46**, 2678 (2021).
8. C.-H. Lu, Y.-J. Tsou, H.-Y. Chen, B.-H. Chen, Y.-C. Cheng, S.-D. Yang, M.-C. Chen, C.-C. Hsu, and A. H. Kung, Optica **1**, 400 (2014).
9. C.-H. Lu, W.-H. Wu, S.-H. Kuo, J.-Y. Guo, M.-C. Chen, S.-D. Yang, and A. Kung, Opt. Express **27**, 15638 (2019).
10. M. Seo, K. Tsendsuren, S. Mitra, M. Kling, and D. Kim, Opt. Lett. **45**, 367 (2020).
11. S. Hädrich, M. Krebs, A. Hoffmann, A. Klenke, J. Rothhardt, J. Limpert, and A. Tünnermann, Light Sci. Appl. **4**, e320 (2015).
12. I. Pupeza, S. Holzberger, T. Eidam, H. Carstens, D. Esser, J. Weitenberg, P. Rußbüldt, J. Rauschenberger, J. Limpert, T. Udem, A. Tünnermann, T. W. Hänsch, A. Apolonski, F. Krausz, and E. Fill, Nat. Photonics **7**, 608 (2013).
13. G. Porat, C. M. Heyl, S. B. Schoun, C. Benko, N. Dörre, K. L. Corwin, and J. Ye, Nat. Photonics **12**, 387 (2018).
14. F. Meyer, N. Hekmat, T. Vogel, A. Omar, S. Mansourzadeh, F. Fobbe, M. Hoffmann, Y. Wang, and C. Saraceno, Opt. Express **27**, 30340 (2019).
15. G. Barbiero, H. Wang, J. Brons, B.-H. Chen, V. Pervak, and H. Fattahi, J. Phys. B **53**, 125601 (2020).
16. I. Pupeza, M. Huber, M. Trubetskov, W. Schweinberger, S. A. Hussain, C. Hofer, K. Fritsch, M. Poetzlberger, L. Vamos, E. Fill, T. Amotchkina, K. V. Kepesidis, A. Apolonski, N. Karpowicz, V. Pervak, O. Pronin, F. Fleischmann, A. Azzeer, M. Žigman, and F. Krausz, Nature **577**, 52 (2020).
17. O. Pronin and J. Brons, *High Power Laser Systems*, M. Harooni, ed. (IntechOpen, 2018), Chap. 5.
18. J. Körner, V. Jambunathan, J. Hein, R. Seifert, M. Loeser, M. Siebold, U. Schramm, P. Sikocinski, A. Lucianetti, T. Mocek, and M. C. Kaluza, Appl. Phys. B **116**, 75 (2014).
19. K. Mak, M. Seidel, O. Pronin, M. Frosz, A. Abdolvand, V. Pervak, A. Apolonski, F. Krausz, J. Travers, and P. St.J. Russell, Opt. Lett. **40**, 1238 (2015).
20. M. Seidel, G. Arisholm, J. Brons, V. Pervak, and O. Pronin, Opt. Express **24**, 9412 (2016).
21. M. Seidel, J. Brons, G. Arisholm, K. Fritsch, V. Pervak, and O. Pronin, Sci. Rep. **7**, 1410 (2017).
22. J. Weitenberg, A. Vernaleken, J. Schulte, A. Ozawa, T. Sartorius, V. Pervak, H.-D. Hoffmann, T. Udem, P. Russbüldt, and T. W. Hänsch, Opt. Express **25**, 20502 (2017).
23. J. Schulte, T. Sartorius, J. Weitenberg, A. Vernaleken, and P. Russbueldt, Opt. Lett. **41**, 4511 (2016).
24. S. Gröbmeyer, K. Fritsch, B. Schneider, M. Poetzlberger, V. Pervak, J. Brons, and O. Pronin, Appl. Phys. B **126**, 159 (2020).
25. K. Fritsch, M. Poetzlberger, V. Pervak, J. Brons, and O. Pronin, Opt. Lett. **43**, 4643 (2018).
26. C.-L. Tsai, F. Meyer, A. Omar, Y. Wang, A.-Y. Liang, C.-H. Lu, M. Hoffmann, S.-D. Yang, and C. J. Saraceno, Opt. Lett. **44**, 4115 (2019).
27. I. Pupeza, D. Sánchez, J. Zhang, N. Lilienfein, M. Seidel, N. Karpowicz, T. Paasch-Colberg, I. Znakovskaya, M. Pescher, W. Schweinberger, V. Pervak, E. Fill, O. Pronin, Z. Wei, F. Krausz, A. Apolonski, and J. Biegert, Nat. Photonics **9**, 721 (2015).
28. J. Zhang, K. Fritsch, Q. Wang, F. Krausz, K. F. Mak, and O. Pronin, Opt. Lett. **44**, 2986 (2019).
29. J. Brons, V. Pervak, D. Bauer, D. Sutter, O. Pronin, and F. Krausz, Opt. Lett. **41**, 3567 (2016).
30. P. He, Y. Liu, K. Zhao, H. Teng, X. He, P. Huang, H. Huang, S. Zhong, Y. Jiang, S. Fang, X. Hou, and Z. Wei, Opt. Lett. **42**, 474 (2017).
31. N. I. Chunosov, "Rezonator2," 2020, http://rezonator.orion-project.org/.
32. J. Hult, J. Lightwave Technol. **25**, 3770 (2007).
33. M. Hanna, X. Délen, L. Lavenu, F. Guichard, Y. Zaouter, F. Druon, and P. Georges, J. Opt. Soc. Am. B **34**, 1340 (2017).
34. H. Pires, M. Baudisch, D. Sanchez, M. Hemmer, and J. Biegert, Prog. Quantum Electron. **43**, 1 (2015).